Eur. Phys. J. B **20**, 65–74 (2001)

THE EUROPEAN PHYSICAL JOURNAL B

EDP Sciences

Remnant Fermi surface in a pseudogap regime of the two-dimensional Hubbard model at finite temperature

T. Saikawa[a] and A. Ferraz[b]

Laboratório de Supercondutividade, Centro Internacional de Física da Matéria Condensada, Universidade de Brasília, CEP 70919-970 Brasília-DF, Brazil

Received 8 September 2000 and Received in final form 20 December 2000

Abstract. A precursor effect on the Fermi surface in the two-dimensional Hubbard model at finite temperatures near the antiferromagnetic instability is studied using three different itinerant approaches: the second order perturbation theory, the paramagnon theory (PT), and the two-particle self-consistent (TPSC) approach. In general, at finite temperature, the Fermi surface of the interacting electron systems is not sharply defined due to the broadening effects of the self-energy. In order to take account of those effects we consider the single-particle spectral function $A(\mathbf{k}, 0)$ at the Fermi level, to describe the counterpart of the Fermi surface at $T = 0$. We find that the Fermi surface is destroyed close to the pseudogap regime due to the spin-fluctuation effects in both PT and TPSC approaches. Moreover, the top of the effective valence band is located around $\mathbf{k} = (\pi/2, \pi/2)$ in agreement with earlier investigations on the single-hole motion in the antiferromagnetic background. A crossover behavior from the Fermi-liquid regime to the pseudogap regime is observed in the electron concentration dependence of the spectral function and the self-energy.

PACS. 71.27.+a Strongly correlated electron systems; heavy fermions – 71.10.Fd Lattice fermion models (Hubbard model, etc.)

1 Introduction

Recently, investigations of the Fermi surface (FS) have been a crucial issue in the study on the high-T_c cuprate superconductors. Angle-resolved photoemission experiments [1,2] have found evidences of deviations from conventional Fermi liquid demonstrating the existence of the pseudogap formation above T_c in the single-particle spectral function and the breakdown of the FS at the so-called "hot-spot" region in the Brillouin zone.

The Fermi surface is an important physical property which characterizes the low temperature behavior of the normal phase of fermion systems. If the stability of the Fermi liquid state is verified, the Luttinger theorem [3] concerning the conservation of the Fermi surface volume holds. However, if the interacting fermion system is in a state close to some instability, the precise definition of both the Fermi liquid and the FS may become uncertain.

Some indications of the deviations from the conventional Fermi surface behavior have already been seen in the two-dimensional (2D) Hubbard model. Quantum Monte Carlo (QMC) simulations [4–6] indicated the change of the FS topology for small hole dopings in the strong coupling regime. This topological change is characterized by the FS closing around $\mathbf{k} = (\pi, \pi)$ despite the (small) hole dopings. In the weak coupling regime of the Hubbard model, using second order perturbation theory, Zlatić *et al.* [7] obtained that the FS changes its topology due to the self-energy effects for small dopings. In contradiction with that, within the same framework of perturbation theory, Halboth and Metzner [8] have shown that the modification of the FS is very small for weak coupling at zero temperature. Thus, even in the weak-coupling regime, the FS of the Hubbard model leads to controversy.

In this paper, we focus on the modification suffered by the FS of the 2D Hubbard model near the antiferromagnetic instability in the weak-coupling regime. The 2D Hubbard model produces several different electronic phases according to the choice of the parameters. For the highly doped case, the system is in the conventional Fermi liquid regime with a well-defined FS. On the other hand, in the ground state at half-filling, the system becomes an antiferromagnetic insulator. Thus, for an appropriate set of parameters, the zero temperature phase transition will take place, and quite probably, the conventional Fermi surface picture is lost before that.

However the long range antiferromagnetic order at half-filling is automatically destroyed at sufficiently high

[a] *Present address*: Dipartimento di Scienze Fisiche "E.R. Caianiello", Università degli Studi di Salerno, 84081 Baronissi (Salerno), Italy
e-mail: tsaikawa@alles.or.jp

[b] *Present address*: Institut de Physique Théorique, Université de Fribourg, Perolles, 1700 Fribourg, Switzerland

temperatures or finite doping. Thus, assuming paramagnetic background at finite temperature we use itinerant approaches such as the second order perturbation theory, the paramagnon theory [9] and also the recently developed two-particle self-consistent approach [10–12] to calculate the effects produced on the FS. Varying the electron concentration, the coupling constant and the temperature, the single-particle spectral function is calculated in all those approaches. In general the FS is well defined for a normal metal at $T = 0$. At finite temperature, however, we cannot define the FS sharply. To describe the counterpart of the Fermi surface at finite temperatures, we introduce the spectral function $A(\mathbf{k}, 0)$ at the Fermi level. The meaning of this quantity is discussed in detail.

We will see that the FS of the Hubbard model at finite temperature shows remarkable modifications. As we approach the antiferromagnetic instability condition, the FS is destroyed at the $(\pi, 0)$ regions in the Brillouin zone. The calculated effective band dispersion indicates that the anisotropic pseudogap and the destruction of the FS are both manifestations of the precursor of the antiferromagnetic instability at half-filling. Besides that, we note that there is a trace of the FS in the pseudogap regime in which there is no effective band dispersion crossing the Fermi level. Also, by varying the electron number per site n, we find that the spectral function and self-energy clearly show a crossover from the Fermi liquid regime at the smaller n to the pseudogap regime near the half-filling.

2 Model

We start with the standard 2D Hubbard Hamiltonian defined by

$$H = -t \sum_{\langle i,j\rangle,\sigma} a^{\dagger}_{i\sigma} a_{j\sigma} + U \sum_{i} n_{i,\uparrow} n_{i,\downarrow} - \mu \sum_{i,\sigma} n_{i,\sigma} \qquad (1)$$

where t is the nearest-neighbor transfer matrix on the square lattice, U is the on-site repulsive coupling constant, μ the chemical potential and $n_{i\sigma} = a^{\dagger}_{i\sigma} a_{i\sigma}$. The Fermi surface can be determined using the single-particle spectra which is calculated with the full Green's function. The spectral function $A(\mathbf{k}, \omega)$ is given in terms of the imaginary part of the retarded Green's function: $A(\mathbf{k}, \omega) = -(1/\pi)\mathrm{Im}G(\mathbf{k}, \omega)$ where $G(\mathbf{k}, \omega)$ is given by

$$G(\mathbf{k}, \omega)^{-1} = \omega + \mathrm{i}\eta - (\varepsilon_{\mathbf{k}} - \mu) - \Sigma(\mathbf{k}, \omega) \qquad (2)$$

with $\varepsilon_{\mathbf{k}} = -2t(\cos k_x + \cos k_y)$ and $\Sigma(\mathbf{k}, \omega)$ is a proper self-energy which is given in the following subsection. The chemical potential μ is determined to be consistent with a given electron concentration n which satisfies

$$n = \sum_{\mathbf{k}\sigma} \int_{-\infty}^{\infty} \mathrm{d}\omega f(\omega) A(\mathbf{k}, \omega) \qquad (3)$$

for fixed values of U/t and T/t. Here $f(\omega)$ is the Fermi distribution function defined by $f(\omega) = 1/[\exp(\omega/T) + 1]$.

Next, we introduce self-energies for three different approaches; the paramagnon theory [9], the second order perturbation theory, and the two-particle self-consistent approach [10–12].

2.1 Paramagnon theory and second order perturbation theory

The paramagnon theory (PT) is probably the simplest way to take account of the magnetic instability in the electronic states qualitatively. In that approach, the divergence of the spin susceptibility in the random phase approximation (RPA) signals the antiferromagnetic instability. At $T = 0$, due to the perfect nesting condition, the real part of the one-loop polarization bubble $\mathrm{Re}\chi_0(\mathbf{q}, 0)$ diverges, and the PT approach cannot be simply applied. χ_0 is given by

$$\chi_0(\mathbf{q}, \nu_m) = \sum_{\mathbf{k}} \frac{f(\varepsilon_{\mathbf{k}+\mathbf{q}} - \mu_0) - f(\varepsilon_{\mathbf{k}} - \mu_0)}{\mathrm{i}\nu_m - (\varepsilon_{\mathbf{k}+\mathbf{q}} - \varepsilon_{\mathbf{k}})} \qquad (4)$$

with $\nu_m = 2m\pi T$ and μ_0 is the chemical potential in the non-interacting case. At non-zero temperature, however, $\mathrm{Re}\chi_0(\mathbf{q}, 0)$ remains finite even at half-filling. Thus, the RPA spin susceptibility does not diverge for suitable small values of the coupling constant U and the system remains in its paramagnetic regime. We perform all calculations in the present paper with suitable choices of the temperature T, the coupling constant U, and the electron concentration n. A zero-temperature version of our approximation has been used by Kampf [13] to calculate the spectral function of the doped Hubbard model. One drawback of the paramagnon theory is that it does predict the antiferromagnetic instability in two dimensions violating in this way the Mermin-Wagner theorem. However, if we avoid this transition regime by working at finite temperatures, as we have shown in our previous work [9], this approach gives the qualitatively correct non-Fermi-liquid energy dependence in the self-energy with the corresponding anisotropic pseudogap in the single-particle spectral function. These results are in general agreement with several other approaches [11,12,14,15]. Moreover, the anisotropy of the pseudogap, which has been observed also in the QMC simulation by Creffield *et al.* [16], was shown in our previous paper.

To derive the self-energy, we use the standard diagram technique by treating the interaction term perturbatively. Since the Hartree-Fock term $Un/2$ is nothing but a constant energy shift, we include it in the chemical potential. The self-energy in the PT framework can be written as

$$\Sigma^{\mathrm{PT}}(\mathbf{k}, \omega_n) = U^2 T \sum_{\nu_m} \sum_{\mathbf{q}} \left[\frac{1}{2}\chi_{\mathrm{c}}(\mathbf{q}, \nu_m) + \frac{3}{2}\chi_{\mathrm{s}}(\mathbf{q}, \nu_m) - \chi_0(\mathbf{q}, \nu_m) \right] G_0(\mathbf{k} + \mathbf{q}, \omega_n + \nu_m) \qquad (5)$$

where $G_0(\mathbf{k}, \omega_n)$ is the non-interacting Green's function with $\omega_n = (2n+1)\pi T$. Here we have introduced the charge

susceptibility by $\chi_c(\mathbf{q},\nu_m) = \chi_0(\mathbf{q},\nu_m)/[1+U\chi_0(\mathbf{q},\nu_m)]$ and the spin susceptibility by $\chi_s(\mathbf{q},\nu_m) = \chi_0(\mathbf{q},\nu_m)/[1-U\chi_0(\mathbf{q},\nu_m)]$. In the angular bracket in equation (5), $\chi_0(\mathbf{q},\nu_m)$ is subtracted to avoid the double counting of the lowest order diagram. $\Sigma(\mathbf{k},\omega)$ in equation (2) is obtained from $\Sigma^{\rm PT}(\mathbf{k},\omega_n)$ by performing an analytic continuation.

In contrast, the self-energy obtained from conventional second order perturbation theory is given by

$$\Sigma^{\rm 2nd}(\mathbf{k},\omega_n) = U^2 T \sum_{\nu_m}\sum_{\mathbf{q}} \chi_0(\mathbf{q},\nu_m) G_0(\mathbf{k}+\mathbf{q},\omega_n+\nu_m). \tag{6}$$

This is equivalent to the lowest order contribution of the self-energy $\Sigma^{\rm PT}(\mathbf{k},\omega_n)$ in the paramagnon theory. Detailed investigation on $\Sigma^{\rm 2nd}(\mathbf{k},\omega_n)$ of the Hubbard model is seen in references [7,8,17].

2.2 Two-particle self-consistent approach

The two-particle self-consistent (TPSC) approach has been developed by Vilk *et al.* [10–12]. This approach can give both the spin and charge structure factors in good quantitative agreement with the results of the quantum Monte Carlo simulations in the Hubbard model [10]. Detailed argument on this approach has been given in their review article [12]. Following their formulation, the self-energy of the single electron Green's function in TPSC approach is given by

$$\Sigma^{\rm TPSC}(\mathbf{k},\omega_n) = \frac{U}{2} T \sum_{\nu_m}\sum_{\mathbf{q}} \left[U_{\rm ch}\chi_{\rm c}^{\rm TPSC}(\mathbf{q},\nu_m) + U_{\rm sp}\chi_{\rm s}^{\rm TPSC}(\mathbf{q},\nu_m)\right] G_0(\mathbf{k}+\mathbf{q},\omega_n+\nu_m) \tag{7}$$

where $\chi_{\rm c}^{\rm TPSC}(\mathbf{q},\nu_m) = \chi_0(\mathbf{q},\nu_m)/[1+U_{\rm ch}\chi_0(\mathbf{q},\nu_m)]$ and $\chi_{\rm s}^{\rm TPSC}(\mathbf{q},\nu_m) = \chi_0(\mathbf{q},\nu_m)/[1-U_{\rm sp}\chi_0(\mathbf{q},\nu_m)]$. The Hartree-Fock term has been absorbed again in the chemical potential. Note the difference of the factor 2 of our definition of χ_0 here from the one in their original papers. The renormalized coupling constants $U_{\rm sp}$ and $U_{\rm ch}$ are determined by solving the self-consistent equations given by

$$T\sum_{\nu_m}\sum_{\mathbf{q}} 2\chi_{\rm s}^{\rm TPSC}(\mathbf{q},\nu_m) = n - 2\langle n_\uparrow n_\downarrow\rangle, \tag{8}$$

$$T\sum_{\nu_m}\sum_{\mathbf{q}} 2\chi_{\rm c}^{\rm TPSC}(\mathbf{q},\nu_m) = n + 2\langle n_\uparrow n_\downarrow\rangle - n^2, \tag{9}$$

and

$$U_{\rm sp} = \frac{4U}{n^2}\langle n_\uparrow n_\downarrow\rangle \cdot \tag{10}$$

Here $\langle n_\uparrow n_\downarrow\rangle$ is the average double occupancy per site.

Note that contrary to the other two methods the Mermin-Wagner theorem is satisfied at any finite temperature in the TPSC approach [10,12]. To review it briefly, let's consider the half-filling case. At half-filling, from equations (10) and (8), we obtain the following self-consistent equation to compute $U_{\rm sp}$:

$$T\sum_{\nu_m}\sum_{\mathbf{q}} \frac{2\chi_0(\mathbf{q},\nu_m)}{1-U_{\rm sp}\chi_0(\mathbf{q},\nu_m)} = 1 - \frac{U_{\rm sp}}{2U} \cdot \tag{11}$$

If $U_{\rm sp}$ always satisfies the condition $1 > U_{\rm sp}\chi_0(\mathbf{Q},0)$, the magnetic instability is not realized, namely the Mermin-Wagner theorem holds. It is convenient to rewrite the above self-consistent equation in terms of two functions $f_1(u)$ and $f_2(u)$ defined by

$$f_1(u) = T\sum_{\nu_m}\sum_{\mathbf{q}} \frac{2\chi_0(\mathbf{q},\nu_m)}{1-u\chi_0(\mathbf{q},\nu_m)} \tag{12}$$

and

$$f_2(u) = 1 - \frac{u}{2U} \cdot \tag{13}$$

The self-consistent equation (11) is equivalent to the relation $f_1(U_{\rm sp}) = f_2(U_{\rm sp})$. Figure 1 shows a schematic plot of $f_1(u)$ and $f_2(u)$ as the functions of u for finite T. The behavior of $f_2(u)$ is trivial. Note that the slope of $f_2(u)$ is in proportion with $1/U$. Using the sum rule of χ_0 given in the appendix, we see $f_1(u=0) = 0.5$. $f_1(u)$ diverges as u approaches $1/\chi_0(\mathbf{Q},0)$. This divergence was proved by Vilk and Tremblay [12]. The intersection of $f_1(u)$ and $f_2(u)$ gives the solution of the self-consistent equation. From the plot, we see that the intersection point always stays within the range $0 < u < 1/\chi_0(\mathbf{Q},0)$ for arbitrary U. Namely, the solution of the TPSC self-consistent equation never violates the Mermin-Wagner theorem.

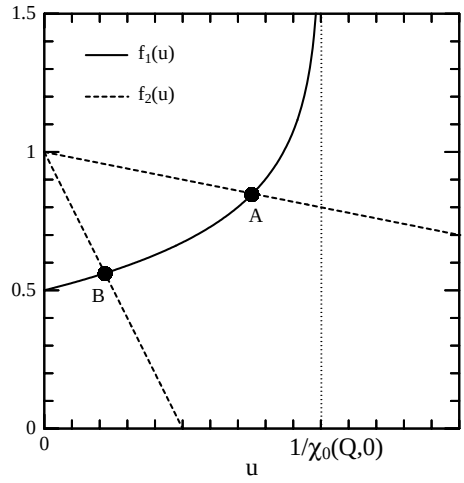

Fig. 1. A schematic plot of the functions $f_1(u)$ and $f_2(u)$. The solid circles A and B indicate the solutions of the equation $f_1(u) = f_2(u)$ for larger U and smaller U, respectively.

3 Fermi surface at finite temperature

Let's consider how to obtain the information on the Fermi surface from the full Green's function given by equation (2) at finite temperature. So far, several different

methods to investigate the FS have been used in the literature. One straightforward way to define the FS is given by the quasiparticle poles of the Green's function through the solutions of $\varepsilon_{\mathbf{k}_\mathrm{F}} - \mu + \mathrm{Re}\Sigma(\mathbf{k}_\mathrm{F}, 0) = 0$. Another way is to use the electron momentum distribution function $n(\mathbf{k})$ defined by $n(\mathbf{k}) = \int_{-\infty}^{\infty} \mathrm{d}\omega f(\omega) A(\mathbf{k}, \omega)$. In this case, the FS is characterized by each $\mathbf{k}$ point associated with a finite discontinuity of $n(\mathbf{k})$. Those definitions give a proper FS at zero temperature. However, at finite temperature, since the imaginary part of the self-energy has a finite value with a non-trivial $\mathbf{k}$ dependence in general, these definitions are not applicable. Another definition is to use $n(\mathbf{k}_\mathrm{F}) = 1/2$. This is not useful to apply for the pseudogap regime since this condition is always satisfied at half-filling and at finite temperature. Maximum slope of $\nabla_\mathbf{k} n(\mathbf{k})$ is also used in the determination of the FS obtained with the angle-resolved photoemission [18,19]. However, because $n(\mathbf{k})$ is obtained from a quantity which is integrated over the energy, it has a maximum slope even if a gap or a pseudogap exists. At finite T the FS is often defined approximately by the $\mathbf{k}$ points at which the effective band dispersion crosses on the Fermi level. The effective band dispersion is obtained from the maximum intensity points of the spectral function.

Strictly speaking, at finite temperature we cannot define a sharp FS because of the broadening effects in the spectral function. However, in principle, the Fermi level can be calculated for any sets of parameters of the system if the number of electrons is known. We therefore use this route to establish the Fermi surface. Taking into account the above consideration on the FS, instead of employing conventional definitions, we consider the electron distribution at the Fermi level. Such distribution can be represented by a single-particle spectral function written as

$$A(\mathbf{k}, 0) = \frac{1}{\pi} \frac{\mid \mathrm{Im}\Sigma(\mathbf{k}, 0) \mid}{[\varepsilon_\mathbf{k} - \mu - \mathrm{Re}\Sigma(\mathbf{k}, 0)]^2 + [\mathrm{Im}\Sigma(\mathbf{k}, 0)]^2} \cdot \quad (14)$$

It is evident that it satisfies a sum-rule $N(0) = \sum_\mathbf{k} A(\mathbf{k}, 0)$ where $N(0)$ is the density of states (DOS) at the Fermi level. $A(\mathbf{k}, 0)$ contains all the information of the single-particle states at the Fermi level and possesses enough information to study the properties of the Fermi surface.

We easily see that $A(\mathbf{k}, 0)$ has the following features, which covers the basic properties of the conventional FS. When the system is described by the conventional Fermi-liquid at zero temperature, we have that

$$A(\mathbf{k}, 0) = \delta(\varepsilon_\mathbf{k} - \mu - \mathrm{Re}\Sigma(\mathbf{k}, 0)) \quad (15)$$

and the peak points of the delta-function trace a sharply defined FS in the $\mathbf{k}$ space. Thus, $A(\mathbf{k}, 0)$ recovers the conventional FS at the ground states. In a Fermi liquid at finite temperature, the spectral function becomes broad around the Fermi level. Quite naturally, $A(\mathbf{k}, 0)$ covers this feature because it has a finite width and it draws a broad trace in the $\mathbf{k}$ space. On the other hand, when the system does not have a spectral weight at all at the Fermi level ($N(0) = 0$) – for instance, an insulating state with a real gap – $A(\mathbf{k}, 0)$ is identically zero for all wave vectors. Thus, $A(\mathbf{k}, 0)$ represents all cases ranging from the well-defined FS to the vanishing FS limit. As a result, $A(\mathbf{k}, 0)$ can be used to trace the evolution of the FS in all cases. Observed Fermi surface in angle-resolved photoemission experiments is extracted from the finite weight of the single particle spectra in the vicinity of the Fermi level. Here too, in this respect, it is meaningful to introduce $A(\mathbf{k}, 0)$ in order to study the FS structure.

As we see from the argument above, the generalized FS at finite temperatures is no longer strictly speaking a *surface* in the momentum space. It is not clear if it could be used as the counterpart of the $T = 0$ FS. This issue could be solved by analogy with what happens to the band dispersion in both non-interacting and interacting systems. The electronic states in the free-fermion system in a lattice is completely described by a non-interacting band dispersion $\omega = E_\mathbf{k} - \mu$. In the interacting system, within certain theoretical treatment of the interaction term, the spectral function $A(\mathbf{k}, \omega)$ contains all the information of the single-particle states, but the (effective) band dispersion cannot fully describe the electronic states. The FS of the non-interacting system is given by $E_\mathbf{k} - \mu = 0$. On the other hand, $A(\mathbf{k}, 0)$ at the Fermi level continues to carry all necessary information concerning the electronic states. As a result it replaces the band dispersion in the description of the electronic states in the interacting system. In the following section of this paper, we use the term, Fermi surface, in this extended sense.

4 Results

Using the self-energies and the Green's functions presented in the previous section, numerical calculations were performed in the same manner as in our previous work [9]. A mesh of about 4000 grids in the first Brillouin zone has been used to compute the momentum integral to obtain the imaginary parts of both charge and spin susceptibilities. A 120×120 mesh on the Brillouin zone has been used to perform the momentum integrations for the self-energies to obtain the Green's functions and the spectral functions.

4.1 Second order perturbation theory

In Figure 2 we show the temperature dependence of DOS calculated using the second order perturbation theory for $U = 4.0t$ and $n = 1.0$. Detailed analyses of the self-energy and the single-particle spectra at finite temperatures and finite dopings have already been done by Zlatić *et al.* [17]. A main temperature dependence in DOS appears only around the Fermi level ($\omega = 0$). We do not see any pseudogap-like structure in DOS in this approximation. At $T = 0.5t$, the maximum of DOS at the Fermi level is broad. For a lower temperature $T = 0.1t$, this maximum becomes a sharp peak.

Figure 3 shows the gray-scale density plot of $A(\mathbf{k}, 0)$ for the corresponding parameters used in Figure 2. As emphasized earlier on, the density plot of $A(\mathbf{k}, 0)$ in

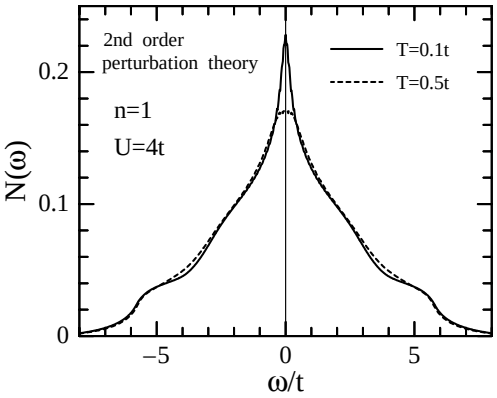

Fig. 2. Temperature dependence of the density of states $N(\omega)$ within the second order perturbation theory for $U = 4.0t$ at half-filling ($n = 1$).

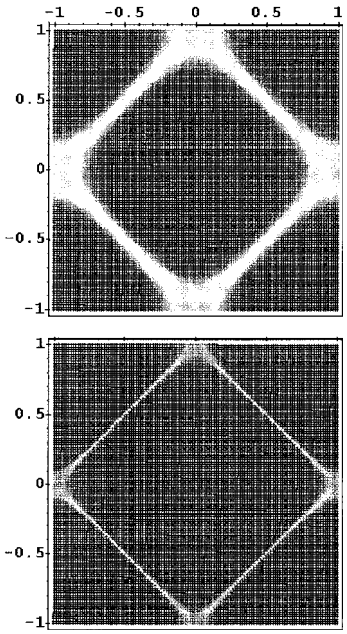

Fig. 3. Spectral intensity $A(\mathbf{k}, 0)$ in the Brillouin zone calculated within the second order perturbation for $U = 4.0t$ at half-filling ($n = 1$). Upper panel for $T = 0.5t$ and lower panel for $T = 0.1t$.

Figure 3 gives a counterpart of the Fermi surface. In this plot, the larger (smaller or zero) intensity of $A(\mathbf{k}, 0)$ is represented by the bright (dark) region and the axes for both k_x and k_y directions are normalized by π. For $T = 0.1t$ (lower panel), a well-defined FS has been obtained. The broadening in the plot for $T = 0.5t$ (upper panel) can be understood as the temperature effect in the self-energy. Thus, within our results, the second order perturbation theory gives the conventional Fermi-liquid-like behavior both in the single-particle spectra and in the FS. Namely, this approach does not explain the breakdown of the Fermi surface. Our calculation has been done at half-filling only whereas the calculation of Zlatic *et al.* [17] is for large doping ($n = 0.8$). They found a topology change of FS, but their choice of parameters may not be entirely suitable for that regime.

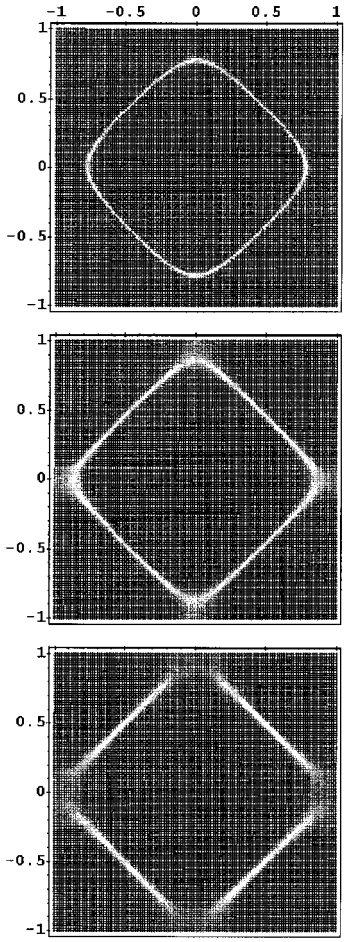

Fig. 4. Spectral intensity $A(\mathbf{k}, 0)$ in the Brillouin zone within the paramagnon theory calculated for various electron concentration n for $U = 2.0t$ at $T = 0.22t$. The upper panel is for $n = 0.8$, the middle panel for $n = 0.9$, and the bottom panel for $n = 1.0$.

4.2 Paramagnon theory

Figure 4 shows the n-dependence of $A(\mathbf{k}, 0)$ for $U = 2.0t$ at $T = 0.22t$ calculated in terms of $\Sigma^{\mathrm{PT}}(\mathbf{k}, \omega_n)$. For $n = 0.8$ (upper panel), a clear and large FS is obtained indicating that the system is in the conventional Fermi liquid phase. For $n = 0.9$ (middle panel), the FS volume is enlarged by the increment of the electron concentration. In addition, the distribution around $(\pi, 0)$ becomes broader. For $n = 1.0$ (lower panel), the FS around $(\pi, 0)$ regions is completely destroyed and there remains well-defined Fermi surface segments only around $(\pi/2, \pi/2)$ regions. This anisotropic destruction of the FS is caused by the anisotropy of the pseudogap formation. The origin of this kind of anisotropic pseudogap has been explained in our previous work [9]. The strong low-energy antiferromagnetic Stoner enhancement in the spin

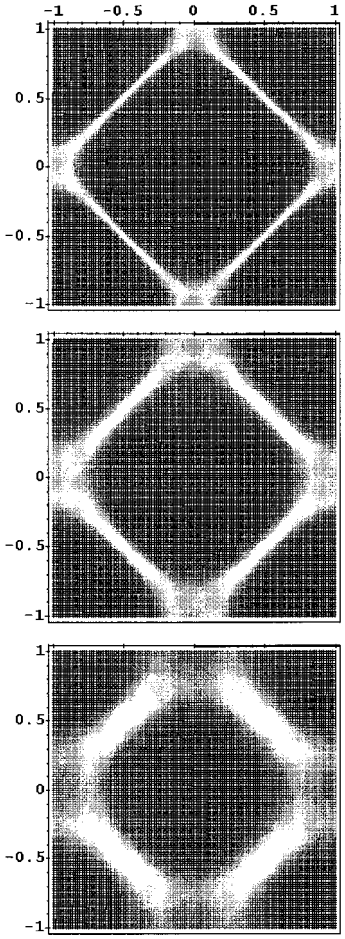

Fig. 5. Spectral intensity $A(\mathbf{k}, 0)$ in the Brillouin zone within the paramagnon theory calculated for various values of U for $T = 0.5$ at half-filling. From top to bottom, $U = 2.0t$, $2.5t$ and $3.0t$, respectively.

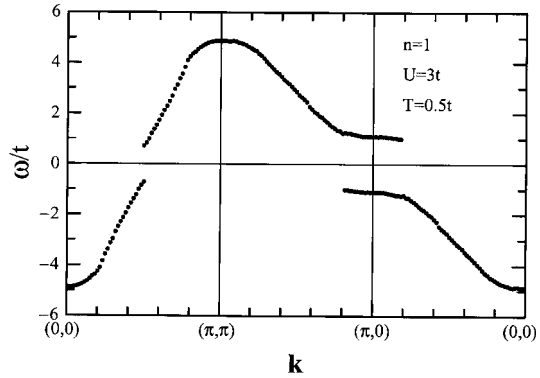

Fig. 6. Effective band dispersion obtained from the spectral function $A(\mathbf{k}, \omega)$ within the paramagnon theory calculated for $U = 3.0t$, $T = 0.5t$ at half-filling.

susceptibility produces the non-Fermi-liquid energy dependence in the fermion self-energy. The momentum dependence of the self-energy is determined by the anisotropy of the band flatness of the non-interacting band dispersion at the Fermi level. As a result of those effects, the pseudogap opens first at the $(\pi, 0)$ regions, and the FS is partially destroyed.

In Figure 5 we plot the U-dependence of the spectral function $A(\mathbf{k}, 0)$ within the paramagnon theory for $T = 0.5t$ at half-filling. For $U = 2.0t$ (upper panel), the FS is rather sharply defined as for the non-interacting case. As U becomes large, the distribution becomes broad and the FS cannot be sharply defined. The tendency for broadening is remarkable in the $(\pi, 0)$ regions. The original structure of the spectral function around $(\pi, 0)$ is almost washed out for $U = 3.0t$. Instead, there is a hollow structure centered on $(\pi, 0)$. The $(\pi/2, \pi/2)$ regions have relatively large intensities.

In Figure 6 we show the effective band dispersion obtained from the main peaks of the spectral functions $A(\mathbf{k}, \omega)$ for the same parameter as the lower panel in Figure 5. The pseudogap around $(\pi, 0)$ is larger than the one at $(\pi/2, \pi/2)$, and segments of the shadow bands [20] can be seen around this point. This result indicates that the top of the effective lower (valence) band is located at $\mathbf{k} = (\pi/2, \pi/2)$. This result is consistent with the earlier investigations of the single-hole motion in the 2D antiferromagnetic background [21]. In Figure 6 it is important to realize that the effective band does not cross the Fermi level. In conventional meaning we cannot define the FS in this regime, but the spectral weight remains at the Fermi level and it forms a very broad remnant Fermi surface structure in the momentum space as we see in the lowermost panel of Figure 5.

4.3 Two-particle self-consistent approach

Figure 7 shows the plot of $A(\mathbf{k}, 0)$ in the TPSC for $U = 4.0t$ at half-filling for $T = 0.5t$ (upper panel) and $T = 0.3t$ (lower panel). Despite the above mentioned difference between the TPSC and PT, both approaches show qualitative agreement with respect to the destruction of FS. The quantitative difference between the two methods is due to the fact that in the PT case the interaction effects are overestimated by the lack of vertex corrections.

In Figure 8 we show the temperature dependence of DOS $N(\omega)$ in the TPSC approach for $U = 4t$ and $n = 1$. As we lower the temperature, the gap-like structure grows at the Fermi energy. That behavior is well correlated with the destruction of the FS observed in Figure 7.

The electron concentration dependence of the spectral intensity $A(\mathbf{k}, 0)$ is shown in Figure 9 for $U = 4t$ and $T = 0.25t$. For $n = 0.85$ (upper panel), the FS is still defined well. At $n = 0.9$, the FS enlarged but in the regions near the Brillouin zone it gets broader. At $n = 0.95$, the FS region near $(\pi, 0)$ becomes very unclear, while the other FS sectors remain relatively well-defined. Again, this indicates the anisotropic breakdown of the Fermi liquid picture on the Fermi level.

In Figure 10 we plot the spectral functions and the self-energies for various electron concentrations for $T = 0.25t$

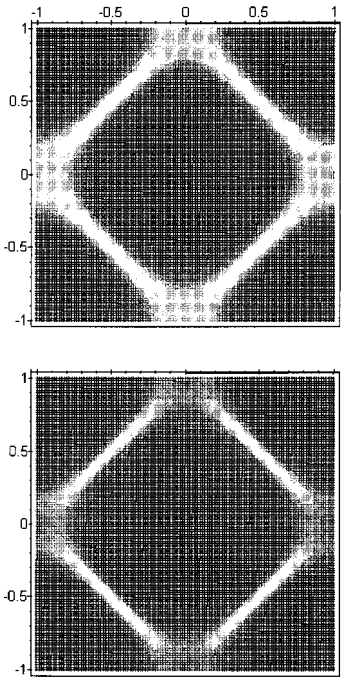

Fig. 7. Temperature dependence of the spectral intensity $A(\mathbf{k}, 0)$ in the Brillouin zone calculated within the two-particle self-consistent approach for $U = 4.0t$ and $n = 1$. Upper panel for $T = 0.5t$ and lower panel for $T = 0.3t$.

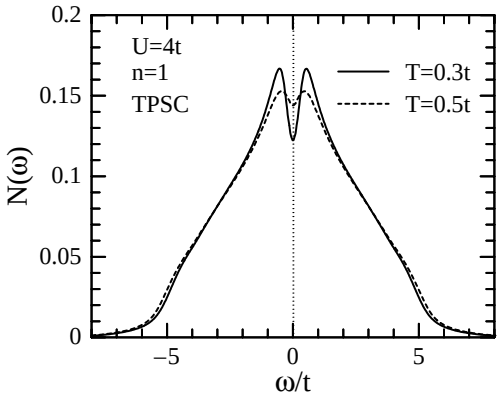

Fig. 8. Temperature dependence of the density of states calculated within the two-particle self-consistent approach for $T = 0.3t$ (solid curve) and $0.5t$ (broken curve) at $U = 4t$ and $n = 1$.

and $U = 4.0t$. For convenience, the momentum $\mathbf{k}_{\mathrm{F}}$ has been assumed to be the same one in the $(1, 0)$ direction on the non-interacting Fermi surface for each n. At $n = 0.8$, the spectral function (a) has a single peak at the Fermi level. This peak corresponds to the conventional Fermi liquid quasiparticle. As increasing n towards half-filling, the peak becomes broader and shifts into the $\omega < 0$ side. On the other hand, a shoulder appears in the $\omega > 0$ side in the spectral function ($n = 0.9$) and in the end this turns into another peak. Thus the quasiparticle is destroyed, and two-peak structure emerges at $n = 1$. The self-energies

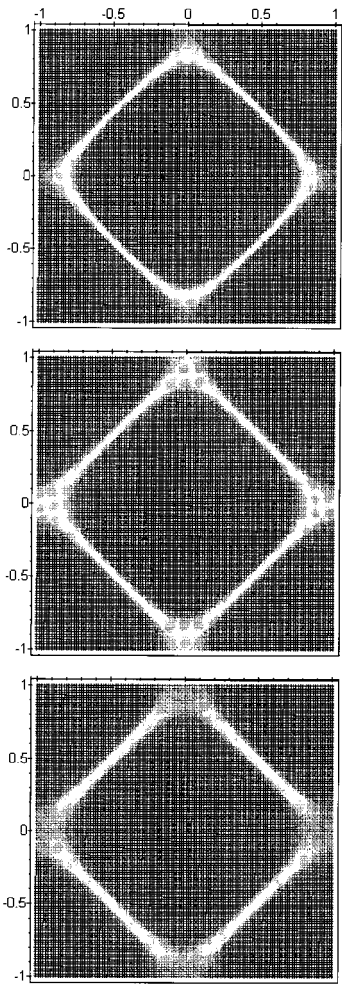

Fig. 9. Electron concentration n dependence of the spectral intensity $A(\mathbf{k}, 0)$ in the Brillouin zone calculated within the two-particle self-consistent approach for $U = 4.0t$ and $T = 0.25$. The upper panel is for $n = 0.85$, the middle panel for $n = 0.9$, and the lower panel for $n = 0.95$.

also show the breakdown of the Fermi liquid picture. In our standard knowledge on the Fermi liquid theory, the real part of the self-energy $\mathrm{Re}\Sigma$ is linear in ω and the slope is negative, and the imaginary part of the self-energy $\mathrm{Im}\Sigma \propto \omega^2$. At $n = 0.8$, the real (b) and imaginary (c) parts of the self-energy show those Fermi liquid like behaviors. As n becomes larger, the self-energy dramatically changes its ω dependence and indicates deviations from the Fermi liquid nature. There are two remarkable features at $n = 1$: (i) the ω dependence of the real part of the self-energy resembles to the spin-density-wave self-energy ($\sim 1/\omega$), (ii) the large negative peak appears in the imaginary part of the self-energy.

5 Discussion and conclusion

We find that the second order perturbation theory fails to show the breakdown of the Fermi surface. The decisive

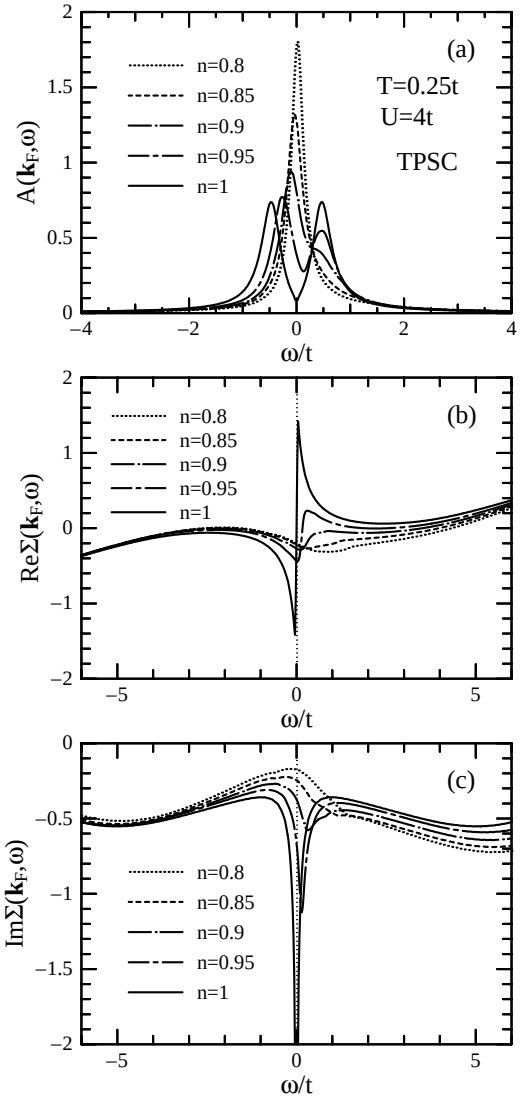

Fig. 10. The spectral function (a), the real part (b) and imaginary part (c) of the self-energy within the two-particle self-consistent approach at $U = 4t$ and $T = 0.25t$ for various electron concentration n. The Fermi momentum in the $(1, 0)$-direction on the non-interacting Fermi surface has been used as $\mathbf{k}_F$ for each n.

difference between the second order perturbation and the other two approaches is the fact that in the former case the Stoner factor is not taken into account in the self-energy. We can immediately see this by comparing the definitions of these self-energies. As we have already mentioned, the Stoner enhancement is important to produce the anomalous energy dependence in the self-energy. If it is combined with the flat-band dispersion the anisotropic pseudogap is formed in the spectral function. Because of this difference in self-energy, the second order perturbation theory FS is well defined and does not show any anomaly even for dopings close to half-filling.

As mentioned in Section 1 there has been some controversy concerning the Fermi surface topology in the 2nd order perturbation theory framework [7,8,17]. This issue was recently discussed by Halboth and Metzner (HM) in [8]. We just want to add that in our calculation we pay attention to the existence of different values of chemical potentials for the non-interacting Green's function and the interacting Green's functions which is renormalized by the self-energy effects. If one uses a fixed value of chemical potential in both cases the conservation of electron number is automatically destroyed. This will in turn produce discrepancies for any finite doping. This does not seem to be taken into account in references [7] and [17].

We discuss next the possibility of the small hole pocket formation in the 2D Hubbard model. Langer *et al.* [22] and Schmalian *et al.* [23], using the fluctuation exchange (FLEX) approximation for the Hubbard model, have investigated how the low-energy electronic states and the FS evolve at finite dopings. They explained [23] one scenario of the formation of the small hole pockets produced by the transfer of the spectral weight from the main band to the shadow band. In the range of the parameters used in our calculation, we have not obtained any sign of the hole pockets or even the "shadow" of the Fermi surface [22], while we observed the segments of the shadow bands in the effective band dispersion. According to the argument in reference [22], the origin of the shadow band is a large imaginary part of the self-energy at the $\mathbf{k} + \mathbf{Q}$ regions rather than another pole in the single-particle Green's function. In their result the imaginary part of the self-energy has a strong momentum dependence. That feature has been seen also in our previous calculation [9]. However, the momentum dependence of $\mathrm{Im}\Sigma(\mathbf{k}, \omega)$ produces the anisotropy of the pseudogap in $A(\mathbf{k}, \omega)$. In both PT and TPSC approach, the origin of the double-peak is clearly associated with the real poles of the full Green's function. Because of this difference, it is natural that our data showed neither the shadow of the FS nor the hole-pockets.

Chubukov and Morr [24] have shown the small hole pocket formation in an analytical investigation based on the nearly antiferromagnetic Fermi liquid approach for the spin-fermion model. Schmalian *et al.* [15] have also obtained the small half-pocket-like segments in the FS for the spin-fermion model. Although both the PT and TPSC approaches are in a different approximation level from their semi-phenomenological model, the importance of the spin-fluctuation is common in both approaches. To compare with their results we need to study the t-t'-U Hubbard model [25] which has the same non-interacting band dispersion including the next-nearest-neighbor hopping t' and to use the Fermi surface topology as they used. If the same mechanism discussed in the present paper works in the t-t'-U model, we can expect to obtain a half closed small FS around the $(\pi/2, \pi/2)$ point.

The single-particle spectrum of the t-J model is equivalent to that of the Hubbard model in the strong coupling limit if we take no consideration of the upper Hubbard band effect. Recently, Dai and Su [26] obtained the destruction of the FS of the t-J model, and the FS for a hole doping clearly shows a topological change of the Fermi surface which is consistent with the results of the QMC

simulations in the large-coupling Hubbard model [4–6]. Putikka *et al.* [27] also showed the violation of the Luttinger theorem in the t-J model.

In the present work which deals with the weak-coupling Hubbard model, we cannot make any decisive statement concerning the validity of the Luttinger theorem although the complete FS structure no longer exists. At half-filling in the arbitrary coupling, the Hubbard model acquires the particle-hole symmetry. Hence, presumably the half-filling Fermi surface (if it exists) cannot show any anomalous topology. As it is well known, in the large coupling regime, the doped Hubbard model have a preformed gap associated with the Mott-Hubbard transition. The energy scale of the preformed gap is of the order of U. The QMC simulations have shown that the doped hole forms a narrow quasiparticle band dispersion on the top of the lower Hubbard band [4–6]. Namely, there is a jump of the Fermi level between the infinitesimal hole and electron dopings. This discontinuity of the Fermi level produces the deviation of the electron-hole symmetry in the electronic states. In the weak-coupling regime, since the effect of the preformed gap at finite temperatures is considerably weak, the electronic states must preserve the electron-hole symmetry for an infinitesimal doping, and the topological change cannot be seen. Thus, the topology change of the FS in the large coupling regime may be a manifestation of the effective violation of the electron-hole symmetry due to the large preformed gap.

In conclusion, we studied the electron distribution $A(\mathbf{k}, 0)$ at the Fermi level for the 2D Hubbard model in the weak-coupling regime. This quantity is useful for the generalization of the conventional Fermi surface concept and can be applied in all circumstances for all ranges of parameters of the Hubbard model at finite temperature. We examined three different itinerant approaches, and found that the second order perturbation theory fails to describe the breakdown of the Fermi surface. In the pseudogap regime, we found that the FS is partially destroyed in PT and TPSC. From the anisotropic pseudogap and also from the destruction of the FS, we observe that the top of the effective valence band is located at $\mathbf{k} = (\pi/2, \pi/2)$. This is in general agreement with previous theoretical studies for a strongly coupled regime [21]. We also investigated the ω dependence of the spectral function and the self-energy on the FS. We showed that there exists only quasiparticle like state for small n. In contrast, as we increase n, we observe a crossover between a Fermi-liquid phase and a spin-density-wave-like regime with the evolution of the precursor pseudogap.

We would like to thank Dr. Z.Y. Weng for stimulating discussions. We also thank Professor H. Kaga for bringing our attention to the references [11,12] and for very useful conversations. This work was supported by the Conselho Nacional de Desenvolvimento Científico e Tecnológico - CNPq and by the Financiadora de Estudos e Projetos - FINEP. Most of the numerical calculations were performed with the supercomputing system at the Institute for Materials Research, Tohoku University, Japan.

Appendix: A sum rule for $\chi_0(\mathbf{Q}, \nu_\mathbf{m})$

In this appendix, we introduce a sum rule for $\chi_0(\mathbf{q}, \nu_m)$ given by

$$T \sum_{\nu_m} \sum_{\mathbf{q}} \chi_0(\mathbf{q}, \nu_m) = \frac{n}{2} \left(1 - \frac{n}{2}\right). \tag{A.1}$$

This holds for arbitrary electron concentrations and for any temperature. It can be proved by calling the definition of $\chi_0(\mathbf{q}, \nu_m)$ given by equation (4). Physically speaking, this sum rule states that the total summation of the particle-hole bubble $\chi_0(\mathbf{q}, \nu_m)$ over $\mathbf{q}$ (in the Brillouin zone) and ν_m is equal to the products of the electron concentration $n/2$ and the hole concentration $1 - (n/2)$ per spin. It is possible to generalize this sum rule for the one-loop diagram given in terms of the full Green's functions $G(\mathbf{k}, \omega_n)$. In this case, the sum rule becomes

$$T \sum_{\nu_m} \sum_{\mathbf{q}} \chi(\mathbf{q}, \nu_m) = \frac{n}{2} \left(1 - \frac{n}{2}\right) \tag{A.2}$$

where

$$\chi(\mathbf{q}, \nu_m) = -T \sum_{\omega_n} \sum_{\mathbf{k}} G(\mathbf{k} + \mathbf{q}, \omega_n + \nu_m) G(\mathbf{k}, \omega_n). \tag{A.3}$$

It can be proved in terms of

$$G(\mathbf{k}, \omega_n) = \int_{-\infty}^{\infty} \frac{\mathrm{d}\omega'}{\pi} \frac{\mathrm{Im} G(\mathbf{k}, \omega')}{\omega' - \mathrm{i}\omega_n}. \tag{A.4}$$

References

1. D.S. Marshall, D.S. Dessau, A.G. Loeser, C-H. Park, A.Y. Matsuura, J.N. Eckstein, I. Bozovic, P. Fournier, A. Kapitulnik, W.E. Spicer, Z.-X. Shen, Phys. Rev. Lett. **76**, 4841 (1996).
2. M.R. Norman, H. Ding, M. Randeria, J.C. Campuzano, T. Yokoya, T. Takeuchi, T. Takahashi, T. Mochiku, K. Kadowaki, P. Guptasarma, D.G. Hinks, Nature **392**, 157 (1998).
3. J.M. Luttinger, J.C. Ward, Phys. Rev. **118**, 1417 (1960); J.M. Luttinger, Phys. Rev. **119**, 1153 (1960).
4. N. Bulut, D.J. Scalapino, S.R. White, Phys. Rev. B **50**, 7215 (1994).
5. R. Preuss, W. Hanke, W. von der Linden, Phys. Rev. Lett. **75**, 1334 (1995); R. Preuss, W. Hanke, C. Gröber, H.G. Evertz, Phys. Rev. Lett. **79**, 1122 (1997).
6. C. Gröber, M.G. Zacher, R. Eder, `cond-mat/9902015`.
7. V. Zlatić, K.D. Schotte, G. Schliecker, Phys. Rev. B **52**, 3639 (1995).
8. C.J. Halboth, W. Metzner, Z. Phys. B **102**, 501 (1997).
9. T. Saikawa, A. Ferraz, Int. Jour. Mod. Phys. B **14**, 2271 (2000).
10. Y.M. Vilk, L. Chen, A.-M.S. Tremblay, Phys. Rev. B **49**, 13267 (1994).

11. Y.M. Vilk, A.-M.S. Tremblay, Europhys. Lett. **33**, 159 (1996).
12. Y.M. Vilk, A.-M.S. Tremblay, J. Phys. I France **7**, 1309 (1997).
13. A.P. Kampf, Phys. Rep. **249**, 219 (1994).
14. J.J. Deisz, D.W. Hess, J.W. Serene, Phys. Rev. Lett. **76**, 1312 (1996).
15. J. Schmalian, D. Pines, B. Stojković, Phys. Rev. Lett. **80**, 3839 (1998); Phys. Rev. B **60**, 667 (1999), `cond-mat/9804129`.
16. C.E. Creffield, E.G. Klepfish, E.R. Pike, S. Sarkar, Phys. Rev. Lett. **75**, 517 (1995).
17. V. Zlatić, S. Grabowski, P. Entel, Phys. Rev. B **56**, 14875 (1997).
18. M. Randeria, G. Jennings, H. Ding, J-C. Campuzano, A. Bellman, T. Yokoya, T. Takahashi, H. Katayama-Yoshida, T. Mochiku, K. Kadowaki, Phys. Rev. Lett. **74**, 4951 (1995).
19. M.C. Schabel, C.-H. Park, A. Matsuura, Z.-X. Shen, D.A. Bonn, Ruixing Liang, W.N. Hardy, Phys. Rev. B **57**, 6107 (1998).
20. A.P. Kampf, J.R. Schrieffer, Phys. Rev. B **42**, 7967 (1990); S. Haas, A. Moreo, E. Dagotto, Phys. Rev. Lett. **74**, 4281 (1995).
21. A.V. Chubukov, D.K. Morr, Phys. Rev. B**57**, 5298 (1998); E. Dagotto, Rev. Mod. Phys. **66**, 763 (1994), and also references therein.
22. M. Langer, J. Schmalian, S. Grabowski, K.H. Bennemann, Phys. Rev. Lett. **75**, 4508 (1995).
23. J. Schmalian, M. Langer, S. Grabowski, K.H. Bennemann, Phys. Rev. B **54**, 4336 (1996).
24. A.V. Chubukov, D.K. Morr, Phys. Rep. **288**, 355 (1997).
25. D. Duffy, A. Moreo, Phys. Rev. B **52**, 15607 (1995); D. Duffy, A. Nazarenko, S. Haas, A. Moreo, J. Riera, E. Dagotto, Phys. Rev. B **56**, 5597 (1997).
26. X. Dai, Z.B. Su, Phys. Rev. Lett. **81**, 2136 (1998).
27. W.O. Putikka, M.U. Luchini, R.R.P. Singh, Phys. Rev. Lett. **81**, 2966 (1998).